



**HAL**  
open science

## Spatiotemporal heterodyne detection

Michael Atlan, Michel Gross

► **To cite this version:**

Michael Atlan, Michel Gross. Spatiotemporal heterodyne detection. *Journal of the Optical Society of America. A Optics, Image Science, and Vision*, 2007, 24, pp.2701-2709. 10.1364/JOSAA.24.002701 . hal-00411788

**HAL Id: hal-00411788**

**<https://hal.science/hal-00411788>**

Submitted on 28 Aug 2009

**HAL** is a multi-disciplinary open access archive for the deposit and dissemination of scientific research documents, whether they are published or not. The documents may come from teaching and research institutions in France or abroad, or from public or private research centers.

L'archive ouverte pluridisciplinaire **HAL**, est destinée au dépôt et à la diffusion de documents scientifiques de niveau recherche, publiés ou non, émanant des établissements d'enseignement et de recherche français ou étrangers, des laboratoires publics ou privés.

# Spatiotemporal heterodyne detection

Michael Atlan<sup>1,\*</sup> and Michel Gross<sup>1</sup>

*<sup>1</sup>Laboratoire Kastler Brossel, École Normale Supérieure,  
Université Pierre et Marie-Curie - Paris 6,  
Centre National de la Recherche Scientifique,  
UMR 8552; 24 rue Lhomond, 75005 Paris, France*

(Dated: August 28, 2009)

## Abstract

We describe a scheme into which a camera is turned into an efficient tunable frequency filter of a few Hertz bandwidth in an off-axis, heterodyne optical mixing configuration, enabling to perform parallel, high-resolution coherent spectral imaging. This approach is made possible through the combination of a spatial and temporal modulation of the signal to reject noise contributions. Experimental data obtained with dynamically scattered light by a suspension of particles in brownian motion is interpreted.

## INTRODUCTION

### Coherent spectral imaging

Coherent spectroscopy enables one to study mechanisms involving dynamic light scattering. The spectral distribution of a monochromatic optical field scattered by moving particles is modified as a consequence of momentum transfer (Doppler broadening). The measurement of the Doppler linewidth of this field (referred as object field) with an optimal sensitivity is crucial, since Doppler conversion yields are typically low.

Optical mixing (or *postdetection filtering*) techniques are derived from RF spectroscopy techniques [1]. They can be grouped in two categories [2, 3] : homodyne and heterodyne schemes. In homodyne mixing (fig. 1(a)), self-beating object light impinges on a  $\Delta\omega_{\text{PM}}$ -bandwidth photodetector (also referred as optical mixer or photo-mixer, PM). To assess a frequency component of the object light, the output of the PM is sent to a spectrum analyser, whose bandwidth  $\Delta\omega_{\text{F}}$  defines the detection resolution. The resulting spectra are proportional to the second-order object field spectral distribution [2, 3]  $S_2(\omega)$ . In heterodyne mixing, sketched in fig. 1(b), the object light is mixed onto a PM with a frequency-shifted reference beam, also called local oscillator (LO). The LO field ( $E_{\text{LO}}$ ) is detuned to provoke a heterodyne beat of the object-LO field cross contributions to the recorded intensity. This beat is sampled by a PM and sent to a spectrum analyser whose bandwidth  $\Delta\omega_{\text{F}}$  defines the apparatus resolution. This scheme enables one to measure the first order object field spectral distribution  $S_1(\omega)$  [2, 3].

In heterodyne optical mixing experiments, the PM bandwidth  $\Delta\omega_{\text{PM}}$  defines the span of the measurable spectrum (usually  $\sim 1$  GHz). The resolution  $\Delta\omega_{\text{F}}$  can be lowered down to the sub Hertz range, which is suitable for, among other applications, spectroscopy of liquid and solid surfaces [4], dynamic light scattering [2] and in vivo laser Doppler anemometry [5]. But these schemes are inadequate for imaging applications, because measurements are done on one point. The absence of spatial resolution has been sidestepped by scanning techniques [6, 7], designed at the expense of temporal resolution.

We present a heterodyne optical mixing detection scheme on an array detector (configuration of fig. 1(b)). Typical array detectors sampling rates seldom run over 1 kHz, failing to provide a bandwidth large enough for most Doppler applications to date. Nevertheless, their strong advantage is to perform a parallel detection over a large number of pixels. We present a spatial and temporal modulation scheme (spatiotemporal heterodyning) that uses the spatial sampling capabilities of an area detector to counterbalance the noise issue of a measurement in heterodyne configuration performed in the low temporal frequency range (e.g. with a typical CCD camera). The issue of using narrow-bandwidth camera PMs is alleviated by detuning the LO field optical frequency accordingly to the desired spectral point of the object field to measure. Post-detection filtering results from a numerical Fourier transform over a limited number of acquired images.

This heterodyne optical mixing scheme on a low frame rate array detector can be used as a filter to analyze coherent light. It has already been used in several applications yet, including the detection of ultrasound-modulated diffuse photons [8, 9], low-light spectrum analysis [10], laser Doppler imaging [11, 12, 13], and dynamic coherent backscattering effect study [14]. The purpose of this paper is to present its mechanism.

### **Time domain description of the fields**

We consider the spatially and temporally coherent light field of a CW, single axial mode laser (dimensionless scalar representation) :

$$E_L(t) = A_L A_t(t) \exp(i\omega_L t + i\phi(t)) \quad (1)$$

where  $\omega_L$  is the angular optical frequency,  $A_L$  is the amplitude of the field (positive constant),  $A_t(t) = 1 + a(t)$ ;  $|a(t)| \ll 1$  describes the laser amplitude fluctuations and  $\phi(t)$  the phase fluctuations. This field shines a collection of scatterers that re-emits the object field (or scattered field), described by the following function :

$$E_O(t) = A_O X_t(t) A_t(t) \exp(i\omega_L t + i\phi(t)) \quad (2)$$

where  $A_O$  is a positive constant and  $X_t(t)$  is the time-domain phase and amplitude fluctuation induced by dynamic scattering of the laser field, i.e. the cause of the object field

fluctuations due to dynamic scattering we intend to study. As in conventional heterodyne detection schemes, a part of the laser field, taken-out from the main beam constitutes the reference (LO) field :

$$E_{\text{LO}}(t) = A_{\text{LO}}A_t(t) \exp(i\omega_{\text{LO}}t + i\phi(t)) \quad (3)$$

where  $A_{\text{LO}}$  is a positive constant. The LO optical frequency is shifted with respect to the main laser beam by  $\omega_{\text{LO}} - \omega_L$  to provoke a tunable temporal modulation of the interference pattern resulting from the mix of the scattered and reference fields. It can be done experimentally by diffracting the reference beam with RF-driven Bragg cells (acousto-optic modulators) for example.

The expression of the light instant intensity impinging on the camera PMs is :

$$i(t) \simeq i_0(\text{Re}[E])^2 \quad (4)$$

where  $i_0$  is a positive constant and  $\text{Re}[E]$  is the real part of the relevant optical complex field  $E$ . The PMs are considered point-like, their antenna properties [15] are out of the scope of this paper. To take into account the frequency filtering implication of finite time-domain integration, the average intensity detected by the square-law camera PMs is :

$$I(t) = I_0 \int_{-\tau_e/2}^{\tau_e/2} (E(t + \tau) + E^*(t + \tau))^2 d\tau \quad (5)$$

where  $I_0$  is a positive constant and  $\tau_e$  the exposure time. In the frequency-domain, this integration corresponds to a sinc-shaped low-pass filter function whose bandwidth (defined as the distance between the peak and the first zero) is  $1/\tau_e$ .

## OPTICAL CONFIGURATION

### Setup

The common name for optical mixing experiments on an array detector is digital holography. The original underlying interference technique was invented to improve electron microscopy resolution and was successfully applied to monochromatic light imaging [16]. Since the availability of lasers and then digital cameras, digital holography [17] has become an integrant part of many coherent imaging schemes, for its propensity to record

both quadratures of an optical field.

The optical configuration we use can be either a lensless Fourier off-axis holography setup [18, 19] or a Fresnel off-axis holography setup [20]. In the lensless setup, sketched in fig. 2, and considered throughout this study, the point source of the spherical reference wave (LO focal point) is located at  $(x'_0, y'_0)$  in the plane of the object to match the average curvature of the object field. An interference pattern is recorded in the camera plane  $(x, y)$ . The reconstruction algorithm used to calculate the spatial distribution of the scattered field in the object plane consists of only one spatial fast Fourier transform (FFT) [19]. This setup is used to avoid the need of a general Fresnel reconstruction algorithm. In the Fresnel setup [20], the LO is a plane wave and the image reconstruction requires the use of numerical lenses and at least two successive spatial domain FFTs [21].

The digital hologram is recorded with the frequency-shifting method introduced in the heterodyne holography technique [22], used in several imaging and detection schemes [8, 9, 10, 12] for its ability to discriminate efficiently a few Doppler-shifted photons, according to their frequency, from background light [8, 10]. The frequency-shifting method was chosen as an accurate [22] dynamic phase-shifting detection scheme. This method is derived from static phase-shifting interferometry [23] applied to phase-shifting holography [24]. It consists of detuning the LO optical frequency with respect to the main laser beam, to provoke a time domain modulation of the intensity pattern resulting from the cross contribution of object and LO fields.

### Spatial and temporal dependencies

Space (subscript s) and time (subscript t) dependencies of  $X$  and  $A$  are noted  $X(x, y, t) = X_s(x, y) \cdot X_t(t)$ ,  $A(x, y, t) = A_s(x, y) \cdot A_t(t)$ . Spatial frequencies (subscript sf) and temporal frequencies (subscript f) reciprocal distributions form Fourier pairs with time domain and spatial domain distributions. We have :

$$Y_f(\omega) = \int_{-T/2}^{T/2} Y_t(t) \exp(-i\omega t) dt \quad (6)$$

and

$$Y_{sf}(\xi, \eta) = \int_{-\Delta x/2}^{\Delta x/2} \int_{-\Delta y/2}^{\Delta y/2} Y_s(x, y)$$

$$\times \exp(-2i\pi(x\xi + y\eta)) dx dy \quad (7)$$

where  $Y$  is the considered distribution,  $T$  is the measurement time,  $\Delta x$  and  $\Delta y$  are the camera sensor widths.

In the lensless Fourier configuration, the LO wave curvature matches the average curvature of the object field. Therefore, the heterodyne interference pattern on the detector is formally *equivalent* [18] to the one that would impinge on the detector under Fraunhofer conditions. Consequently, we can consider the (far field diffraction) equivalent situation where the LO wave is a tilted plane wave in the detector plane and the object field distribution is the Fourier transform of its spatial distribution in the object plane. The object and LO complex optical fields take the following form:

$$\begin{aligned} E_O(x, y, t) = & \\ & A_O X_s(x, y) A_s(x, y) \\ & \times X_t(t) A_t(t) \exp(i\omega_L t + i\phi(t)) \end{aligned} \quad (8)$$

$$\begin{aligned} E_{LO}(x, y, t) = & \\ & A_{LO} A_s(x, y) \exp(2i\pi(x\xi_0 + y\eta_0)) \\ & \times A_t(t) \exp(i\omega_{LO} t + i\phi(t)) \end{aligned} \quad (9)$$

where  $\xi_0 = x'_0/(\lambda d)$  and  $\eta_0 = y'_0/(\lambda d)$ . The tilt angle of the reference field leads to the phase factor  $\exp(2i\pi(x\xi_0 + y\eta_0))$ . The detected intensity is :

$$\begin{aligned} I(x, y, t) = & \\ I_0 \int_{-\tau_e/2}^{\tau_e/2} [ & E_O(x, y, t + \tau) + E_{LO}(x, y, t + \tau) \\ & + E_O^*(x, y, t + \tau) + E_{LO}^*(x, y, t + \tau)]^2 d\tau \end{aligned} \quad (10)$$

Expression 10 has 16 terms among which 10 vanish because of the presence of optical frequencies in the phase factors [4], which lead to oscillations outside the detection bandwidth.

It can be rewritten as :

$$\begin{aligned} I(x, y, t)/I_0 = & \\ & A_O A_{LO} I_1(x, y) \cdot I_1(t) \end{aligned}$$

$$\begin{aligned}
& +A_{\text{O}}A_{\text{LO}} I_2(x, y) \cdot I_2(t) \\
& +A_{\text{LO}}^2 I_3(x, y) \cdot I_3(t) \\
& +A_{\text{O}}^2 I_4(x, y) \cdot I_4(t)
\end{aligned} \tag{11}$$

where the time-domain fluctuations of the intensity are :

$$\begin{aligned}
I_1(t) &= \int_{-\tau_e/2}^{\tau_e/2} X_t(t + \tau) |A_t(t + \tau)|^2 \\
&\times \exp(-i(\omega_{\text{LO}} - \omega_{\text{L}})(t + \tau)) \, d\tau
\end{aligned} \tag{12}$$

$$\begin{aligned}
I_2(t) &= \int_{-\tau_e/2}^{\tau_e/2} X_t^*(t + \tau) |A_t(t + \tau)|^2 \\
&\times \exp(i(\omega_{\text{LO}} - \omega_{\text{L}})(t + \tau)) \, d\tau
\end{aligned} \tag{13}$$

$$I_3(t) = \int_{-\tau_e/2}^{\tau_e/2} |A_t(t + \tau)|^2 \, d\tau \tag{14}$$

$$I_4(t) = \int_{-\tau_e/2}^{\tau_e/2} |X_t(t + \tau)|^2 |A_t(t + \tau)|^2 \, d\tau \tag{15}$$

and the spatial contributions to the intensity take the following form :

$$\begin{aligned}
I_1(x, y) &= \\
&|A_s(x, y)|^2 X_s(x, y) \exp(2i\pi(x\xi_0 + y\eta_0))
\end{aligned} \tag{16}$$

$$\begin{aligned}
I_2(x, y) &= \\
&|A_s(x, y)|^2 X_s^*(x, y) \exp(-2i\pi(x\xi_0 + y\eta_0))
\end{aligned} \tag{17}$$

where  $\xi_0 = x'_0/(\lambda d)$  and  $\eta_0 = y'_0/(\lambda d)$ .

$$I_3(x, y) = |A_s(x, y)|^2 \tag{18}$$

$$I_4(x, y) = |X_s(x, y)|^2 |A_s(x, y)|^2 \tag{19}$$

Temporal and spatial dependencies can be treated separately. Eq. 11 has four terms : the first two are object-LO field cross terms. The third and fourth terms correspond to the LO and object fields self beating contributions. The two first spatial contributions,  $I_1(x, y)$  &  $I_2(x, y)$  will be referred as heterodyne, and  $I_3(x, y)$  &  $I_4(x, y)$  as homodyne, as well as their

temporal counterparts.

An assumption about the relative amplitudes of the fields is usually made [2] : the object field amplitude is much lower than the LO field amplitude (heterodyne regime) :

$$A_O \ll A_{LO} \tag{20}$$

This assumption leads to neglecting the object field self-beating contribution, because its relative amplitude with respect to the cross terms is  $A_O/A_{LO} \ll 1$ . Additionally, in usual optical mixing schemes on photodiodes, laser amplitude fluctuations are neglected (i.e.  $a(t) = 0$ ) [2, 4], since the measurement is done with detectors whose bandwidth is large enough to make this assumption valid, as the detection is made at higher frequencies. But with a slow PM such as a CCD camera, the frequency-domain noise resulting from these fluctuations is not negligible.

A sequence of  $n$  images is sampled and leads to a data cube  $I(x, y, t)$ , acquired for a given detuning frequency  $\omega_{LO} - \omega_L$ . To make a spatial map of one frequency component of the object field, a demodulation in the time and spatial domains is performed. As we will see, the heterodyne holography scheme allows encoding of the spectral and spatial information about the object field in the reciprocal space of the data cube, and it also allows spatial discrimination of the self beating terms from the object-LO field cross terms.

### **SIGNAL DEMODULATION IN THE TIME DOMAIN.**

$I_1$  and  $I_2$  are referred as the heterodyne terms (modulated at the detuning frequency  $\omega_{LO} - \omega_L$ , on purpose). They correspond to the object and LO field cross terms.  $I_3$  and  $I_4$  are referred as the homodyne terms (not *explicitly* modulated at the detuning frequency). These terms correspond to the object field (and the LO field) self beating intensity contributions.

To measure a spectral component of the object field,  $n$  samples of  $I(x, y, t)$  along the time axis are acquired. These images are used to calculate both quadratures of the object field by making a time domain demodulation consisting of calculating the first harmonic

component ( $I(x, y, \omega_S/n)$ ) of the recorded sequence. This method is also used in temporal heterodyne inline holography [25, 26]. The relation between the result of this demodulation and the temporal frequency content of the object field is investigated.

### First heterodyne term

Let's consider the first heterodyne term :

$$I_1(t) = F(t) \exp(-i(\omega_{LO} - \omega_L)t) \quad (21)$$

where  $F(t)$  is :

$$F(t) = \int_{-\tau_e/2}^{\tau_e/2} |A_t(t + \tau)|^2 X_t(t + \tau) \times \exp(-i(\omega_{LO} - \omega_L)\tau) d\tau \quad (22)$$

According to eq. 22,  $F(t)$  corresponds to the result of the application of a bandpass filter (of center frequency  $\omega_{LO} - \omega_L$  and bandwidth  $1/\tau_e$ ) on  $X_t(t)$ .

To *demodulate* the signal, the first harmonic ( $\omega_S/n$ ) of the sampled image sequence is calculated by FFT :

$$I_1(\omega_S/n) = \sum_{k=1}^n I_1(t_k) \exp(-2ik\pi/n) \quad (23)$$

where  $t_k = 2k\pi/\omega_S$  is the instant at which the  $k^{\text{th}}$  image is recorded. We have :

$$I_1(\omega_S/n) = \sum_{k=1}^n F(t_k) \exp(-i(\omega_{LO} - \omega_L)t_k) \times \exp(-2ik\pi/n) \quad (24)$$

$I_1(\omega_S/n)$  is a measurement of the  $\omega_{LO} - \omega_L + \omega_S/n$  frequency component of  $F(t)$  (the corresponding instrumental bandwidth is  $\omega_S/n$ ). Eq. 22 and 24 show that the spectral resolution of this measurement should either be limited by the measurement time ( $n/\omega_S$ ) and/or the spectral distribution of the amplitude noise of the laser.

### Second heterodyne term

The assessment of the quantity  $I_2(\omega_S/n)$  is straightforward :

$$I_2(\omega_S/n) = \sum_{k=1}^n F^*(t_k) \exp(i(\omega_{LO} - \omega_L)t_k)$$

$$\times \exp(-2ik\pi/n) \quad (25)$$

where  $F^*(t)$  is the complex conjugate of  $F(t)$  defined by eq. 22. Equations 22 and 25 define the action of two successive selective filters on  $X_t(t)$ . The filters bandwidths are the same as the ones introduced to describe the first heterodyne term. Their action is presented and compared to their counterparts appearing in the first homodyne term in the next section.

### Bandpass filtering

If we neglect the contribution of the amplitude fluctuations  $A_t(t)$  to the laser linewidth, the impulse response functions for the first and second heterodyne terms ( $B_+(\omega_{LO} - \omega_L)$  and  $B_-(\omega_{LO} - \omega_L)$  respectively) calculated by setting  $X_t(t) = 1$  in expressions 24, 25 and 22 take the form :

$$B_{\pm}(\omega_{LO} - \omega_L) = \text{sinc}((\omega_{LO} - \omega_L) \tau_e) \times \sum_{k=1}^n \exp(-2ik\pi/n) \exp(\mp 2ik\pi \frac{\omega_{LO} - \omega_L}{\omega_S}) \quad (26)$$

The instrumental response  $|B_{\pm}(\omega_{LO} - \omega_L)|^2$  was measured experimentally, by analyzing light backscattered by a static object. Data points of this instrumental response are plotted as a function of the detuning frequency in fig. 3. The square amplitude of the function described by eq. 26 is represented in fig. 4. Although their shape is similar, the dynamic range of the theoretical filter is wider than the measured response. The difference is attributed to the linewidth contribution of laser intensity fluctuations. One important thing to remark about those instrumental responses is their dissymmetry.

$|I_1(\omega_S/n)|^2$  and  $|I_2(\omega_S/n)|^2$  are calculated to represent quantities homogenous to the optical power of the object field. This power is proportional to the object field power resulting from the integration of its spectral density in the  $B_{\pm}$  windows. We call these distributions *signal* (or *true image*) and *ghost* (or *twin image*), respectively.  $B_{\pm}$  describe bandpass filters of width  $\Delta\omega_F = \omega_S/n$ , centered on  $\omega_{LO} - \omega_L \pm \omega_S/n$ . Consequently, this scheme allows one to measure the  $\omega_{LO} - \omega_L \pm \omega_S/n$  frequency components of the object field fluctuations  $X_t(t)$ .

If we set the detuning frequency to :

$$\omega_{\text{LO}} - \omega_{\text{L}} = \Delta\omega - \omega_{\text{S}}/n \quad (27)$$

the signal will correspond to the  $\Delta\omega$  frequency component of the field and the ghost area to the  $\Delta\omega + 2\omega_{\text{S}}/n$  component. We have  $|I_1(\omega_{\text{S}}/n)|^2 \approx S_1(\Delta\omega)$  and  $|I_2(\omega_{\text{S}}/n)|^2 \approx S_1(\Delta\omega + 2\omega_{\text{S}}/n)$ . The corresponding frequency diagram is sketched in fig. 5.

### **Homodyne terms. LO and object fields self beating**

In usual heterodyne monodetection schemes, self-beating contributions are considered as an unavoidable noise component, which can actually be neglected in a high bandwidth PM detection scheme. When using low frequency PMs such as camera pixels, these homodyne contributions (defined by eqs. 14 and 15) have to be taken into account. We show in the next section how these terms are filtered-out spatially in the detection process.

## **SIGNAL DEMODULATION IN THE SPATIAL DOMAIN. FILTERING OF SELF-BEATING CONTRIBUTIONS**

### **Heterodyne contributions**

The precious advantage of holography is to allow sampling of the diffracted object complex field (in phase and amplitude), whose spatial distribution in the detector plane is described by the  $X_{\text{s}}(x, y)$  function. The time domain demodulation presented in the previous section enables one to measure the spatial distribution of a tunable frequency component of the object field, in amplitude and phase (i.e. both quadratures). Thus, after temporal demodulation, the actual complex distributions defined by eqs. 16 and 17 are available.

As a result of the off-axis configuration, the object-LO field cross terms (or heterodyne contributions) carry phase factors  $\exp(\pm 2i\pi(x\xi_0 + y\eta_0))$ . The relative distance between each point  $(x', y')$  of the object (described by  $X_{\text{s}}(x', y')$ ) and the LO focal point  $(x'_0, y'_0)$  in the object plane is encoded in a set of parallel (complex) Young's fringes in the detector plane  $(x, y)$ . The periods of these fringes are  $(\lambda d/(x' - x'_0))$  and  $\lambda d/(y' - y'_0)$ . Their spatial

frequencies are noted  $\Delta\xi_0 = (x' - x'_0)/(\lambda d)$  and  $\Delta\eta_0 = (y' - y'_0)/(\lambda d)$ .

In Fraunhofer conditions, the relative distances between each point of the object  $(x', y')$  and the LO focal point  $(x'_0, y'_0)$  are proportional to the spatial frequencies of the hologram in the camera plane  $(\xi, \eta)$ . We have :

$$|X_{\text{sf}}(\xi = x'/(\lambda d), \eta = y'/(\lambda d))|^2 \propto |X_s(x', y')|^2 \quad (28)$$

Hence the requirement for only one spatial Fourier transform to reconstruct the image [19, 21, 27] , i.e. to calculate the spatial distribution  $|X_s(x', y')|^2$ .

The laser amplitude noise leads to flat-field fluctuations in the camera plane. The spatial frequencies distribution of this noise is considered to be a centered dirac :

$$\begin{aligned} & \int_{-\Delta x/2}^{\Delta x/2} \int_{-\Delta y/2}^{\Delta y/2} |A_s(x, y)|^2 \\ & \times \exp\left(-\frac{2i\pi}{\lambda d}(xx' + yy')\right) dx dy \\ & \approx \delta(x', y') \end{aligned} \quad (29)$$

this assumption is implicit in lensless digital holography. The spatial frequency content of  $I_1(x, y)$  , assessed by a FFT, takes the following form :

$$\begin{aligned} |I_1(\xi = x'/(\lambda d), \eta = y'/(\lambda d))|^2 & \propto \\ |X_s(x' - x'_0, y' - y'_0)|^2 & \end{aligned} \quad (30)$$

The ghost distribution is :

$$\begin{aligned} |I_2(\xi = x'/(\lambda d), \eta = y'/(\lambda d))|^2 & \propto \\ |X_s(x'_0 - x', y'_0 - y')|^2 & \end{aligned} \quad (31)$$

In the lensless configuration, both signal and ghost spatial distributions are focused in the same reconstruction plane. Eqs. 30 and 31 define two spatial distributions flipped one with respect to the other and shifted away by  $\pm(x'_0, y'_0)$  from the center of the reconstructed hologram. The spatial instrumental response width corresponds to less than the distance between two adjacent pixels in the reconstructed image [27]; its contribution is neglected.

## Homodyne contributions

The object and LO self beating contributions  $I_3$  and  $I_4$  are not encoded in the spatial complex fringe system which results from the interference of the object field and the off-axis LO. Under the assumption of a perfect flat-field amplitude noise (eq. 29), the spatial frequency content of eqs. 18 and 19 take the form :

$$I_3(\xi = x'/(\lambda d), \eta = y'/(\lambda d)) \propto \delta(x', y') \quad (32)$$

and

$$I_4(\xi = x'/(\lambda d), \eta = y'/(\lambda d)) \propto X_s(x', y') * X_s^*(x', y') \quad (33)$$

These terms are restituted inline : they are centered on  $(x' = 0, y' = 0)$  in the hologram reconstructed in the object plane. This enables one to discriminate them spatially from off-axis heterodyne contributions.

## EXPERIMENTS

In previous publications [11, 12, 13], the spatiotemporal heterodyne detection technique was used to perform parallel imaging. Here, we will focus our attention on the temporal domain. We will study in particular how measured frequency spectra are affected by the camera frame rate, exposure time, and total measurement time.

### Setup and data acquisition details

The experimental setup, which is sketched in Fig.2, has been described previously [10, 11, 12, 13]. The light source is a Sanyo DL-7140-201 diode laser ( $\lambda = 780$  nm, 50 mW for 95 mA of current), the camera is a PCO Pixelfly digital CCD camera (12 bit, frame rate  $\omega_S/(2\pi) \simeq 12.5$  Hz, exposure time  $\tau_e \leq 2\pi/\omega_S = 80$  ms, with  $1280 \times 1024$  pixels of  $6.7 \times 6.7 \mu\text{m}$ ), and the frequency shifter is a set of two acousto-optic modulators AOM1 and AOM2 (Crystal Technology;  $\omega_{\text{AOM}1,2} \simeq 80$  MHz). A neutral density is used to control the LO beam intensity. The sample is a  $1 \text{ cm} \times 1 \text{ cm} \times 5 \text{ cm}$  rectangular PMMA transparent cell filled with a diluted suspension of latex spheres in water (Polybead: Polyscience Inc.,

diameter  $0.48 \mu\text{m}$ , undiluted concentration: 2.62% solids-latex). The Polybead suspension is diluted by a factor  $\simeq 9$  (0.5 ml of undiluted suspension + 4 ml of water). A rectangular aperture ( $7 \text{ mm} \times 3 \text{ cm}$ ) located just in front of the cell removes the parasitic light diffused along cell sides. The aperture delimiting the imaged side of the cell is located at a distance  $d \simeq 39 \text{ cm}$  of the camera. This sample is observed in transmission and the spectrum of the light dynamically scattered by the latex spheres in brownian motion is measured by sweeping the AOM1 frequency so that the detuning frequency  $\omega_{\text{LO}} - \omega_{\text{L}}$  is swept from 0 to 16 kHz in 81 frequency points (200 Hz step). For each frequency point a sequence of 32 consecutive CCD frames is recorded to the PC computer hard disk. For each frequency sweep,  $32 \times 81 = 2592$  images are recorded.

### Data analysis

A first experiment consists of acquiring data with 3 frequency sweeps with  $\tau_e = 80 \text{ ms}$ ,  $\tau_e = 20 \text{ ms}$  and  $\tau_e = 5 \text{ ms}$ . For each frequency point, a  $n = 4$  phase demodulation is performed by using either 4, 8, 16 or the complete set of 32 recorded images. When more than 4 images are used, a first  $n = 4$  phase demodulation is done with images 1 to 4, which is followed by a second demodulation with images 5 to 8, and so on. The complex signal resulting from the demodulation of each set of 4 images is then summed to get the final demodulation result. The total measurement time of one frequency point vary from 320 ms ( $4 \times 80 \text{ ms}$ ) to 2.6 s ( $32 \times 80 \text{ ms}$ ), while the total exposure time vary from 20 ms ( $4 \times \tau_e$  with  $\tau_e = 5 \text{ ms}$ ) to 2.6 s ( $32 \times \tau_e$  with  $\tau_e = 80 \text{ ms}$ ).

Fig. 6 represents the resulting images of the rectangular aperture, illuminated in transmission via the diffusing cell, for an exposure time  $\tau_e = 80 \text{ ms}$ , and for a detuning frequency  $(\omega_{\text{LO}} - \omega_{\text{L}})/(2\pi)$  of 0 Hz (a), 400 Hz (b), 4000 Hz (c) and 8000 Hz (d). The images are k-space images obtained by FFT of the hologram measured in the CCD plane and  $n = 4$  phase demodulation with 4 images per frequency point. They are displayed in arbitrary logarithmic scale. The true image (signal) of the rectangular aperture is the region 1 in fig. 6(a). This distribution is the spectral component of the object field of frequency  $\omega_{\text{L}} - \omega_{\text{S}}/n$ . The twin image (ghost) of the aperture is the region 3. In accordance with eq. 30 and 31, it is symmetric with respect to the center (tag 2) of the k-space plane

(null spatial frequency). The twin image corresponds to the  $\omega_L + \omega_S/n$  spectral component. Increasing the detuning frequency  $\omega_{LO} - \omega_L$ , the true and twin images of the aperture become darker and darker. Nevertheless, they are still visible for a 8000 Hz offset. One can notice that for null detuning (fig. 6(a)) some statically scattered parasitic light is detected out of the aperture image (region 4). This parasitic light is no more detected when the frequency offset is non zero (images (b) to (d)).

To perform a quantitative analysis of the signal, we have summed the signal intensity along the columns of the images represented on Fig.6, from line 312 to line 712 (horizontal dashed lines on Fig.6(a)). These traces are represented on fig. 7. The true image corresponds to region 1, the twin image to region 2. Regions 3 and 4 correspond to the background signal. As mentioned in [8, 10], this background signal is due to the shot-noise on the LO. Taking into account the heterodyne gain, the background signal corresponds to an optical signal of one photo electron per pixel for the whole measurement sequence. The background signal provides here a very simple absolute calibration for the optical signal diffused by the sample. Here, in the center of the aperture, the sample diffused signal is about 3.5 times the background i.e. 3.5 photo electron per pixel.

### **Spectra of Doppler-broadened light in the kHz range**

From the reconstructed images (Fig.6), we have calculated the shape of the first order spectrum of the diffused object field. To get these spectra, we have calculated the sum of the area of the true image and twin image areas (regions 1 and 2 in the traces of fig. 7), and subtracted the background (regions 3 and 4 in fig. 7). Fig. 8 and Fig. 9 show brownian frequency spectra of the light dynamically scattered through the cell. These curves have been normalized by the area under the raw lineshapes.

Data was collected for detuning frequencies up to 16 kHz, much larger than the heterodyne receiver bandwidth (0.4 Hz for curve (d), reciprocal of the 2.6 s measurement time). The shape of the spectrum does not depend on the number of images used to perform the demodulation, as we can see in Fig. 8. In the range of exposure times  $\tau_e$  (of one frame) used for the measurement, the shape of the spectra reported on fig. 9 does vary with  $\tau_e$  for the

following values of the latter : 5 ms (curve c), 20 ms (curve b), and 80 ms (curve a). Fig.8 and Fig.9, which exhibit the same lineshape, show that these spectra do not depend on the total exposure time, which varies from 20 ms (Fig. 9(c)) to 2.6 s (Fig. 8(d)). One must notice that these results are valid because the width of the spectrum ( $\simeq 2.5$  kHz half width) is large compared to the instrumental response. In all the presented results, the instrumental response is always smaller than  $1/\tau_e \leq 200$  Hz (width of the sinc factor in Eq.26).

Additionally, we measured the first order spectrum of the object field in fixed instrumental conditions (4-phase demodulation, exposure time  $\tau_e = 80$  ms) to study different samples. The scattering parameters of the suspension were changed in the following manner : the latex beads concentration was halved from one measurement to another. The four Doppler lineshapes reported on fig. 10 correspond to latex volumic fractions ranging from  $2.9 \times 10^{-3}$  (curve a) to  $3.6 \times 10^{-4}$  (curve d).

## DISCUSSION

The presented technique uses and goes beyond the concept of time-average holography. In time-averaged holography, the detector, whose exposure time  $\tau_e$  is large, behaves as a low-pass filter of bandwidth  $1/\tau_e$ . It selects the field components  $E_O(\omega)$  whose frequencies  $\omega = \omega_L + \Delta\omega$  are close to  $\omega_{LO}$ , i.e. which satisfy  $|\Delta\omega|\tau_e < 1$ . This low-pass filtering effect is used to study vibrating objects like musical instruments [28] by imaging the regions which are not moving or which move with a given phase and velocity. In the first case (selection of the non moving regions), the LO beam is not shifted in frequency [29, 30]. In the second case (moving regions), the LO beam is modulated at the object vibration frequency [31, 32] (which, in the temporal frequency domain, corresponds to the generation of adequate LO frequency sidebands).

Our scheme enables detection of a tunable frequency component of the light with a sharp bandwidth defined by the inverse of the acquisition time of a sequence of  $n$  images. But reading-out an optical beat at typically low camera frame rates is difficult in practice in the case of a weak-amplitude object field, because the low frequency part of the temporal frequency spectrum is highly noisy : it contains LO and object field self-beating contribu-

tions. To discriminate the signal from these noise contributions, a lensless Fourier off-axis configuration is used to encode, in a Young fringe system, the distribution of relative positions of object points with respect to the reference point. This scheme allows to reconstitute the object field spatial distribution in the Fourier reciprocal space of the detection plane. Having recourse to an off-axis configuration to sample the heterodyne optical beat enables spatial frequency discrimination of the *heterodyne* terms (object and reference light cross terms) carrying useful information from the object and reference light self-beating terms carrying what turns out to be unwanted information. Time domain and spatial domain modulation/demodulation schemes present strong similarities. Equation 16 is the spatial counterpart of eq. 21. Signal and ghost distributions are beating at  $\pm\omega_s/n$  in time domain. This beating enables to perform a  $n$ -phase temporal demodulation of the recorded image sequence to assess object and ghost fields in quadrature. Since these complex fields are spatially modulated because of the off-axis interferometry configuration (according to eqs. 16 and 17), their distributions in the object plane are translated by  $\pm(x'_0, y'_0)$  (respectively) away from  $(0,0)$ -centered homodyne contributions. This is highly valuable since it allows one to filter them out spatially.

## CONCLUSION

The presented scheme, based on heterodyne optical mixing onto a parallel detector used as a selective frequency filter, is particularly suited to high resolution spectral imaging. A tunable frequency component of the object field is acquired at a time. The camera finite exposure time and the finite measurement time lead to a frequency domain bandpass filter, whose width is the reciprocal of the measurement time. The small dissymmetry of the frequency domain instrumental response should be taken into account in quantitative measurements. The available range of frequency shifts at which measurements can be made is not limited to the photo-mixer bandwidth (contrary to wide-field laser Doppler [33]), and benefits from heterodyne amplification. The measurement is sensitive : thanks to the off-axis holographic setup, the self beating intensity contributions resulting from laser instabilities and scattered light self interference within the camera bandwidth can be efficiently filtered-out. The propensity to separate spatially cross terms intensity contributions from self beating contributions lies in the use of a spatial heterodyne method.

The presented scheme is the association of a spatial and a temporal heterodyne detection.

Both temporal and spatial resolution are potentially high. This combination is enabled by a wide field measurement performed at one frequency point at a time. The data transfer rate bottleneck implies a tradeoff between the number of pixels in the image and the frame rate of the detector, which should be guided by the application needs in terms of temporal, spectral and spatial resolution. In a few words, combining a spatiotemporal modulation and demodulation of a coherent probe light allows one to achieve a sensitive wide field detection of a tunable Hertz-resolved spectral component with an array detector.

The authors acknowledge support from the French National Research Agency (ANR) and from Paris VI University (BQR grant).

---

\* Corresponding author: atlan@lkb.ens.fr

- [1] A. T. Forrester. Photoelectric mixing as a spectroscopic tool. *J. Opt. Soc. Am.*, 51:253, 1961.
- [2] B. J. Berne and R. Pecora. *Dynamic Light Scattering*. Dover, 2000.
- [3] Judith C. Brown. Optical correlations and spectra. *American Journal of Physics*, 51(11):1008–1011, 1983.
- [4] DS Chung, KY Lee, and E Mazur. Fourier-transform heterodyne spectroscopy of liquid and solid surfaces. *Applied physics. B, Lasers and optics*, 64:1, 1997.
- [5] MD Stern, DL Lappe, PD Bowen, JE Chimosky, GA Holloway, HR Keiser, and RL Bowman. Continuous measurement of tissue blood flow by laser-doppler spectroscopy. *American journal of physiology*, 232(4):H441, 1977.
- [6] TJH Essex and PO Byrne. A laser doppler scanner for imaging blood flow in skin. *J Biomed Eng*, 13(3):189, 1991.
- [7] J. D. Briers. Laser doppler, speckle and related techniques for blood perfusion mapping and imaging. *Physiological Measurement*, 22:R35–R66, 2001.
- [8] M. Gross, P. Goy, and M. Al-Koussa. Shot-noise detection of ultrasound-tagged photons in ultrasound-modulated optical imaging. *Optics Letters*, 28:2482–2484, 2003.

- [9] M. Atlan, B.C. Forget, F. Ramaz, A.C. Boccara, and M. Gross. Pulsed acousto-optic imaging in dynamic scattering media with heterodyne parallel speckle detection. *Opt. Lett.*, 30(11):1360–1362, 2005.
- [10] M. Gross, P. Goy, B.C. Forget, M. Atlan, F. Ramaz, A.C. Boccara, and A.K. Dunn. Heterodyne detection of multiply scattered monochromatic light with a multipixel detector. *Opt. Lett.*, 30(11):1357–1359, 2005.
- [11] M. Atlan and M. Gross. Laser doppler imaging, revisited. *Review of Scientific Instruments*, 77(11), 2006.
- [12] M. Atlan, M. Gross, T. Vitalis, A. Rancillac, B. C. Forget, and A. K. Dunn. Frequency-domain, wide-field laser doppler in vivo imaging. *Optics Letters*, 31(18), 2006.
- [13] M. Atlan, M. Gross, and J. Leng. Laser doppler imaging of microflow. *Journal of the European Optical Society - Rapid publications*, 1:06025–1, 2006.
- [14] Max Lesaffre, Michael Atlan, and Michel Gross. Effect of the photon’s brownian doppler shift on the weak-localization coherent-backscattering cone. *Physical Review Letters*, 97(3):033901, 2006.
- [15] A.E. Siegman. The antenna properties of optical heterodyne receivers. *Applied Optics*, 5(10):1588, 1966.
- [16] D. Gabor. A new microscopic principle. *Nature*, 161:777–778, 1948.
- [17] J. W. Goodman and R. W. Lawrence. Digital image formation from electronically detected holograms. *Applied Physics Letters*, 11(3):77–79, 1967.
- [18] George W. Stroke. Lensless fourier-transform method for optical holography. *Applied Physics Letters*, 6(10):201–203, 1965.
- [19] Christoph Wagner, Sonke Seebacher, Wolfgang Osten, and Werner Juptner. Digital recording and numerical reconstruction of lensless fourier holograms in optical metrology. *Applied Optics*, 38:4812–4820, 1999.
- [20] U. Schnars. Direct phase determination in hologram interferometry with use of digitally recorded holograms. *Journal of Optical Society of America A.*, 11(7):2011, 1994.
- [21] U. Schnars and W. P. O. Juptner. Digital recording and numerical reconstruction of holograms. *Meas. Sci. Technol.*, 13:R85–R101, 2002.
- [22] F. LeClerc, L. Collot, and M. Gross. Numerical heterodyne holography with two-dimensional photodetector arrays. *Optics Letters*, 25(10):716–718, 2000.

- [23] Katherine Creath. Phase-shifting speckle interferometry. *Applied Optics*, 24(18):3053, 1985.
- [24] I. Yamaguchi and T. Zhang. Phase-shifting digital holography. *Optics Letters*, 18:31, 1997.
- [25] Guy Indebetouw and Prapong Klysubun. Space–time digital holography: A three-dimensional microscopic imaging scheme with an arbitrary degree of spatial coherence. *Applied Physics Letters*, 75(14):2017–2019, 1999.
- [26] G. Indebetouw and P. Klysubun. Spatiotemporal digital microholography. *Optical Society of America Journal A*, 18:319–325, February 2001.
- [27] Thomas M. Kreis. Frequency analysis of digital holography. *Optical Engineering*, 41(4):771–778, 2002.
- [28] N. Demoli and I. Demoli. Dynamic modal characterization of musical instruments using digital holography. *Opt. Express*, 13:4812–4817, 2005.
- [29] Pascal Picart, Eric Moisson, and Denis Mounier. Twin-sensitivity measurement by spatial multiplexing of digitally recorded holograms. *Applied Optics*, 42(11):1947–1957, 2003.
- [30] R. L. Powell and K. A. Stetson. Interferometric vibration analysis by wavefront reconstruction. *J. Opt. Soc. Am.*, 55:1593, 1965.
- [31] C. C. Aleksoff. Time average holography extended. *Appl. Phys. Lett*, 14:23, 1969.
- [32] O. J. Lokberg. Espi- the ultimate holographic tool for vibration analysis. *J. Acoust. Soc. Am.*, 55:1783, 1984.
- [33] A. Serov, B. Steinacher, and T. Lasser. Full-field laser doppler perfusion imaging monitoring with an intelligent cmos camera. *Opt. Ex.*, 13(10):3681, 2005.

## LIST OF FIGURE CAPTIONS

1. Coherent spectral detection schemes : homodyne (a) and heterodyne (b) optical mixing. PM : photomixer (square-law detector). SA : spectrum analyzer.  $E_O$  object field.  $E_{LO}$  : local oscillator field.  $S_1, S_2$  : first and second order object field spectral distributions.
2. Off-axis lensless Fourier configuration for heterodyne holography.  $L$  : laser.  $M$  : mirror.  $BS$  : beam splitter.
3. Measurement of the temporal frequency instrumental response. Camera framerate :  $\omega_S/2\pi = 8$  Hz. Exposure time :  $\tau_e = 124$  ms.  $n = 4$ . Representation of instrumental responses for the true image (signal) and the twin image (ghost), in dB. Horizontal axis : detuning frequency  $(\omega_{LO} - \omega_L)/(2\pi)$ , in Hz. Squares : signal (first heterodyne term). Circles : ghost (second heterodyne term).
4. Squared amplitude of the instrumental response defined by eq. 26. Camera framerate :  $\omega_S/2\pi = 8$  Hz. Exposure time :  $\tau_e = 124$  ms.  $n = 4$ . Representation of  $10 \log_{10}[|B_{\pm}(\omega_{LO} - \omega_L)|^2]$ , in dB. Horizontal axis : detuning frequency  $(\omega_{LO} - \omega_L)/(2\pi)$ , in Hz. Dotted line :  $B_+$ . Continuous line :  $B_-$ .
5. Frequency diagram of heterodyne terms spectral components in the case where the detuning frequency is set to  $\omega_{LO} - \omega_L = \Delta\omega - \omega_S/n$ .
6. Images ( $1024 \times 1024$  pixels) of the sample for  $(\omega_{LO} - \omega_L)/(2\pi)$  equal to 0 Hz (a), 400 Hz (b), 4000 Hz (c) and 8000 Hz (80 ms image exposure time, 4-image demodulation. Arbitrary logarithmic scale display.
7. Traces obtained by summation along columns of Fig.6(a) to (d) intensities. Curves a to d correspond to a detuning frequency  $(\omega_{LO} - \omega_L)/(2\pi)$  equal to 0 Hz (a), 400 Hz (b), 4000 Hz (c) and 8000 Hz (d). Horizontal scale is the image horizontal pixel index. Vertical scale is in linear arbitrary units.
8. Frequency spectra of the light diffused through a suspension of latex particles in brownian motion. Exposure time is  $\tau_e = 80$  ms. Demodulation is performed with 4 (a), 8 (b),

- 16 (c) and 32 (d) images. Horizontal axis is the detuning frequency  $(\omega_{\text{LO}} - \omega_{\text{L}})/(2\pi)$  in kHz. Vertical scale is in linear arbitrary units. The four curves overlap.
9. Spectra measured with exposure time  $\tau_e = 80$  ms (a), 20 ms (b), 5 ms (c), and 4-image demodulation. Note that curve (a) the same as Fig.8 (4 images and 80 ms). Vertical scale is in linear arbitrary units. The three curves overlap.
10. Frequency lineshapes of the light diffused through the cell for different concentrations of latex spheres. Exposure time is  $\tau_e = 80$  ms. 4-image demodulation. Horizontal axis is the detuning frequency  $(\omega_{\text{LO}} - \omega_{\text{L}})/(2\pi)$  in kHz. Vertical scale is in linear arbitrary units. Volumic concentration of latex beads :  $2.9 \times 10^{-3}$  (a),  $1.5 \times 10^{-3}$  (b),  $7.3 \times 10^{-4}$  (c), to  $3.6 \times 10^{-4}$  (d).

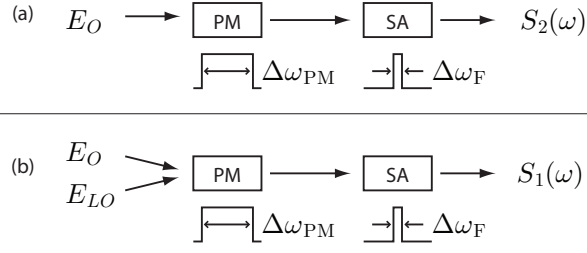


FIG. 1: Coherent spectral detection schemes : homodyne (a) and heterodyne (b) optical mixing. PM : photomixer (square-law detector). SA : spectrum analyzer.  $E_O$  object field.  $E_{LO}$  : local oscillator field.  $S_1, S_2$  : first and second order object field spectral distributions.

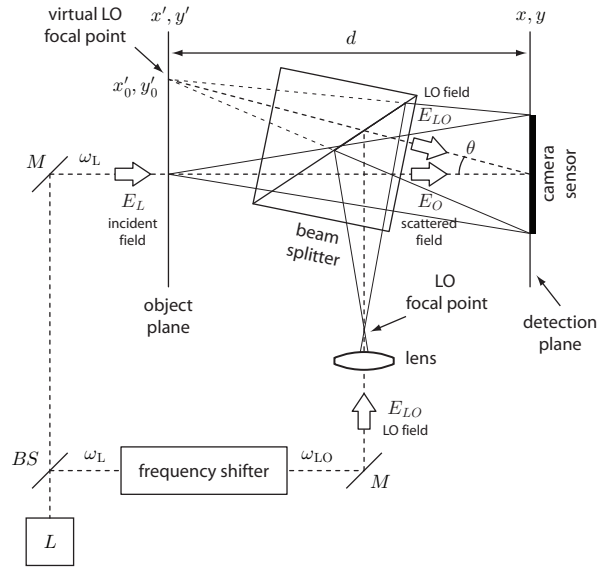


FIG. 2: Off-axis lensless Fourier configuration for heterodyne holography.  $L$  : laser.  $M$  : mirror.  $BS$  : beam splitter.

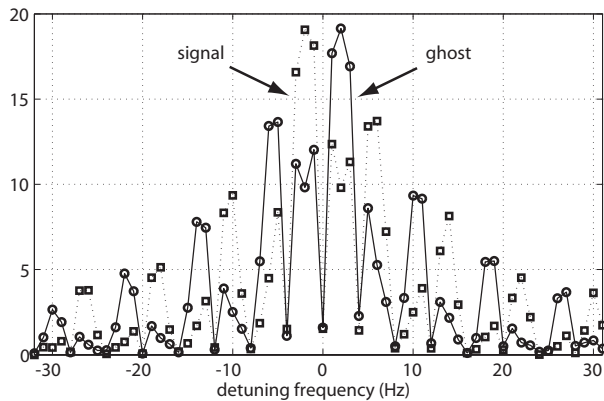


FIG. 3: Measurement of the temporal frequency instrumental response. Camera framerate :  $\omega_S/2\pi = 8$  Hz. Exposure time :  $\tau_e = 124$  ms.  $n = 4$ . Representation of instrumental responses for the true image (signal) and the twin image (ghost), in dB. Horizontal axis : detuning frequency  $(\omega_{LO} - \omega_L)/(2\pi)$ , in Hz. Squares : signal (first heterodyne term). Circles : ghost (second heterodyne term).

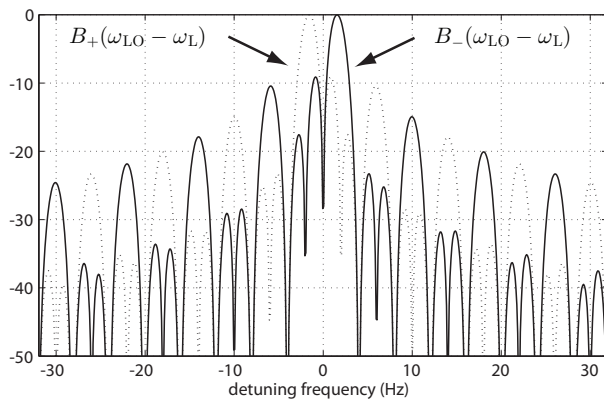


FIG. 4: Squared amplitude of the instrumental response defined by eq. 26. Camera framerate :  $\omega_S/2\pi = 8$  Hz. Exposure time :  $\tau_e = 124$  ms.  $n = 4$ . Representation of  $10 \log_{10}[|B_{\pm}(\omega_{LO} - \omega_L)|^2]$ , in dB. Horizontal axis : detuning frequency  $(\omega_{LO} - \omega_L)/(2\pi)$ , in Hz. Dotted line :  $B_+$ . Continuous line :  $B_-$ .

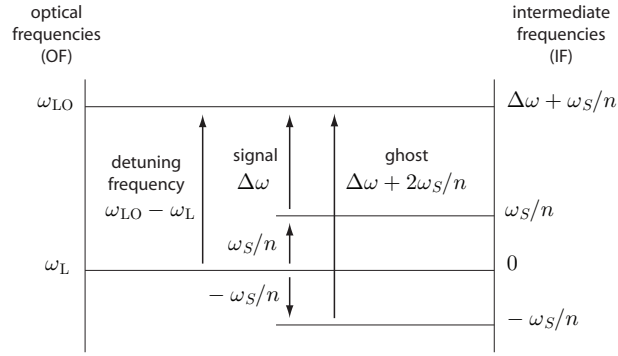


FIG. 5: Frequency diagram of heterodyne terms spectral components in the case where the detuning frequency is set to  $\omega_{LO} - \omega_L = \Delta\omega - \omega_S/n$ .

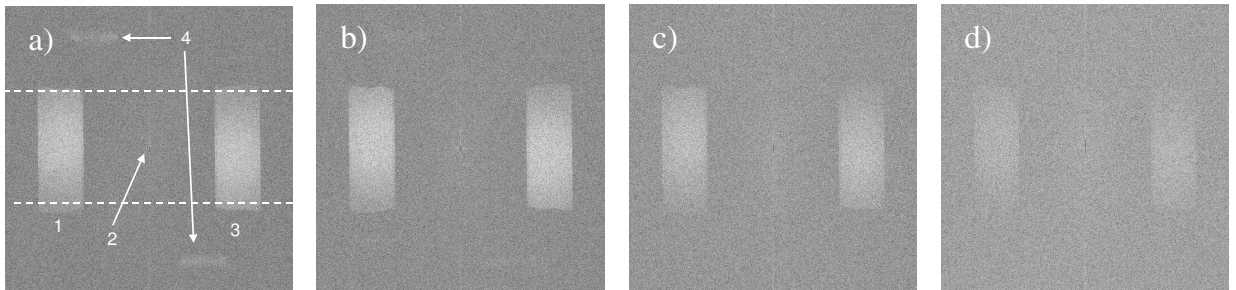


FIG. 6: Images ( $1024 \times 1024$  pixels) of the sample for  $(\omega_{LO} - \omega_L)/(2\pi)$  equal to 0 Hz (a), 400 Hz (b), 4000 Hz (c) and 8000 Hz (80 ms image exposure time, 4-image demodulation). Arbitrary logarithmic scale display.

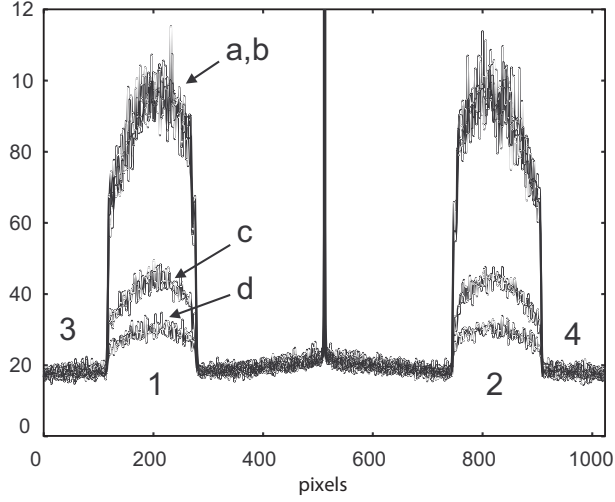


FIG. 7: Traces obtained by summation along columns of Fig.6(a) to (d) intensities. Curves a to d correspond to a detuning frequency  $(\omega_{LO} - \omega_L)/(2\pi)$  equal to 0 Hz (a), 400 Hz (b), 4000 Hz (c) and 8000 Hz (d). Horizontal scale is the image horizontal pixel index. Vertical scale is in linear arbitrary units.

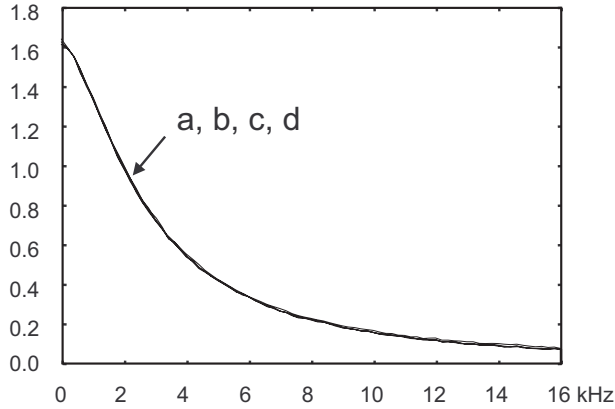


FIG. 8: Frequency spectra of the light diffused through a suspension of latex particles in brownian motion. Exposure time is  $\tau_e = 80$  ms. Demodulation is performed with 4 (a), 8 (b), 16 (c) and 32 (d) images. Horizontal axis is the detuning frequency  $(\omega_{LO} - \omega_L)/(2\pi)$  in kHz. Vertical scale is in linear arbitrary units. The four curves overlap.

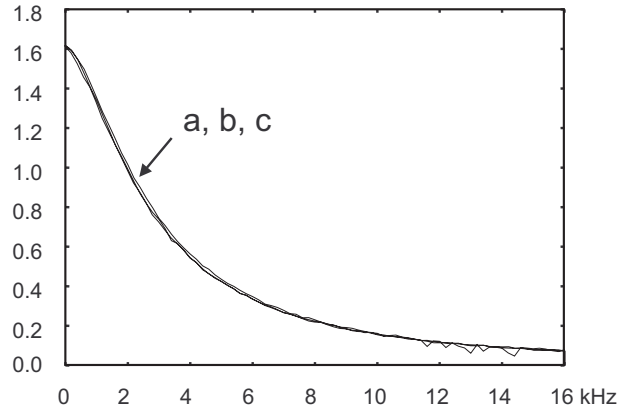


FIG. 9: Spectra measured with exposure time  $\tau_e = 80$  ms (a), 20 ms (b), 5 ms (c), and 4-image demodulation. Note that curve (a) the same as Fig.8 (4 images and 80 ms). Vertical scale is in linear arbitrary units. The three curves overlap.

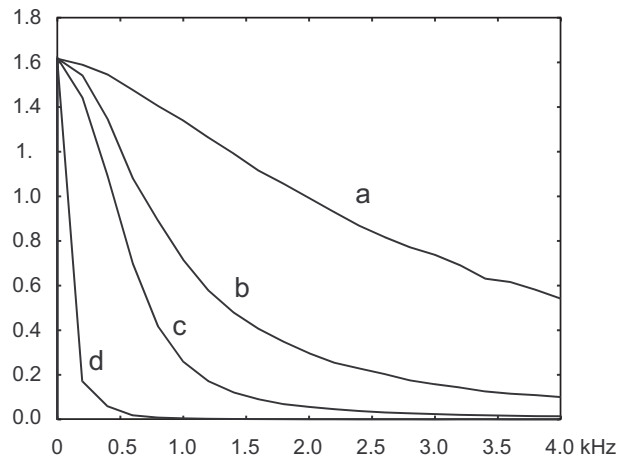


FIG. 10: Frequency lineshapes of the light diffused through the cell for different concentrations of latex spheres. Exposure time is  $\tau_e = 80$  ms. 4-image demodulation. Horizontal axis is the detuning frequency  $(\omega_{LO} - \omega_L)/(2\pi)$  in kHz. Vertical scale is in linear arbitrary units. Volumic concentration of latex beads :  $2.9 \times 10^{-3}$  (a),  $1.5 \times 10^{-3}$  (b),  $7.3 \times 10^{-4}$  (c), to  $3.6 \times 10^{-4}$  (d).